

# Compatibility of Sun Position Models and 3-D Topographic Data for Prediction of Shadow Zones

Ajay Dashora and Bharat Lohani

**Abstract**—Solar energy is increasingly being used for a large number of human activities. Determination of shadow or illuminated zones, and, subsequently, the quantity of insolation are important inputs to these applications. Sun position model and topographic data form the basic input for shadow determination. A variety of sun position models and topographic data, with varying degrees of accuracies, are being used. This paper presents a methodology for determining the compatibility between any particular sun position model and a topographic data, thus leading to an optimal combination in their use. As the interaction of sun rays and 3-D terrain results in shadow, the compatibility is analyzed analytically and graphically by modeling error propagation in determination of shadow coordinates using 3-D topographic data and sun position algorithms. Results are shown for two distant locations.

**Index Terms**—Accuracy of 3-D data, compatibility, sun position model.

## I. INTRODUCTION

THE sun is a source of renewable energy and an important natural resource for the hygienic and healthy living conditions on the planet. The main advantage of solar energy is its no or minimal impact on the environment. Therefore, exploitation of solar energy for applications like photovoltaic (PV) solar panels, artificial trees [1], residential buildings, and vertical farming [2] is in high demand. Remote sensing-based methods for estimating, modeling, and forecasting the sun irradiance for PV applications has already been explored extensively [3]–[6]. Furthermore, Web-based services are also developed that share the information of available local sun potential in an area for commercial use and public awareness [7], [8]. All of these applications require prediction of sun position (i.e., its azimuth and elevation angles) with certain accuracy. Not only the sun position but also the relative orientation and location of the receiving surfaces play a significant role, especially for urban applications [e.g., building integrated PV (BIPV), vertical farming, sun light, solar cooking, and in-house electronic appliances]. Therefore, this demands highly accurate 3-D data (geometry) of the urban features, e.g., buildings, trees, ground, and other obstructions.

The 3-D structure of an obstruction controls the illuminated and shadowed zones in an urban environment. Therefore, the

calculation of shadow coordinates is always dictated by the accuracies (or quality) of 3-D data of obstructions and the sun position. The limitation posed by the quality of 3-D terrain data has been highlighted in numerous researches of large and small extent. In earlier attempts, the given topographic terrain was generalized by a rough digital elevation model (DEM), as the accurate 3-D data were either not available or considered to be unimportant [9]. The approximation in terrain representation was also due to the fact that, for detailed 3-D data acquisition in large areas, the conventional topographic survey methods proved to be time-consuming, labor-intensive, and commercially available. Furthermore, if high-resolution data were available, they were limited to only 2-D representation and rarely had information on 3-D aspects of buildings or trees which are important for shadow prediction [9].

Various modern survey techniques, including total station, laser scanning (LiDAR), and GPS, are used these days to capture the 3-D structure of urban environment with varying accuracy (millimeter to decimeter) and cost. Data derived from satellite images and interferometry are also in use, though have coarser accuracy. Using airborne and terrestrial LiDAR survey (ALS and TLS) techniques, it is possible to collect comprehensive 3-D data with desired fine details for a large area in less time. Moreover, LiDAR data, due to their dense, accurate, and fast coverage, are considered to be better for representing 3-D structures in comparison to the conventional data. Several algorithms and methodologies have been reported in [10]–[13] for efficient generation of solar energy by computing the solar potential for building roof and facade, by the use of LiDAR data.

A sun position model utilizes an observer's location on the earth surface (i.e., longitude and latitude) to determine the sun azimuth and elevation in local geodetic plane (LG) system with certain accuracy. Sun position algorithms like Cooper's, Spencer's, Pitmann and Vanthull's, and Walraven's, which are commonly used for most of the solar engineering applications [14], are categorized as less accurate. On the other hand, the Astronomic Almanac's Algorithm (AAA) [15], the PSA Algorithm [14], SPA Algorithm [16], and the ENEA Algorithm [17] provide more accurate prediction and are preferred for sophisticated solar applications of dynamic nature (e.g., sun tracking mechanism).

In an engineering project, the selection of resources (hardware or software) is generally governed by the fact that the desired project accuracy should be obtainable at minimum financial cost. Consequently, before selection of resources for shadow prediction, it is necessary to evaluate the resources, i.e., 3-D data and sun algorithm, against this criterion. The condition of minimum cost of all resources employed can be defined as

Manuscript received December 20, 2011; revised February 08, 2012; accepted April 10, 2012. Date of publication May 18, 2012; date of current version November 14, 2012.

The authors are with the Department of Civil Engineering, Indian Institute of Technology Kanpur, Kanpur, U.P., India (corresponding author, e-mail: blohani@iitk.ac.in).

Digital Object Identifier 10.1109/JSTARS.2012.2195478

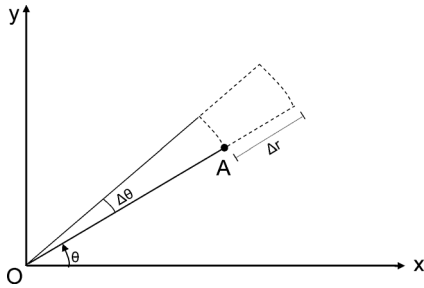


Fig. 1. Propagated error in the location of point A.

“financial compatibility.” Therefore, for shadow prediction, the cost should consist of the sum of the costs contributed by each resource, i.e., sun model and 3-D data. It is understood that using 3-D data and sun algorithm shadow coordinates due to an obstruction can be computed. The computed coordinates will have errors in two orthogonal directions on the LG plane, with their quantum being governed by the chosen resources. The “positional compatibility” is said to be achieved if these two directional components are of same magnitude, thereby avoiding bias or skewness in the uncertainty. The “resource compatibility” can be defined when both resources involved in shadow prediction contribute equally or in comparable quantities to the total error. Unilateral increase in the accuracy of one resource is not justified, as it does not necessarily lead to significant increase in total accuracy while it may increase the cost in a significant manner. From the above discussion, it is clear that resource selection for shadow prediction is primarily governed by the financial compatibility and total accuracy achievable. The positional compatibility is desirable. The resource compatibility, though desirable, is rather superseded by the financial compatibility.

In view of the availability of a large range of accuracies for sun position models and 3-D data, it is important that their financial compatibility along with accuracies (or precision) should be investigated in order to choose an optimal combination for predicting illuminated and shadowed zones. In view of this, this paper will arrive at methodology to determine financial compatibility, the maximum error, and its positional compatibility. Hence, this paper aims at answering the question that which sun position algorithm should be an appropriate match in view of the quality of available 3-D data and vice versa.

This paper uses the term “shadow,” “shadow zone,” or “shadow coordinates,” though the technique proposed is equally valid for illuminated area or their coordinates. This paper first discusses the approach adopted for error propagation of shadow coordinates and subsequently presents the compatibility criteria. The results are shown graphically for better understanding.

## II. CONCEPTUALIZATION AND MATHEMATICAL FORMULATION

### A. Concept of Compatibility and Cost

Consider point A in 2-D space which is located at radial distance  $r$  and angle  $\theta$  from the origin O (Fig. 1). Observational

random errors in distance ( $\Delta r$ ) and angle ( $\Delta\theta$ ) may displace the point A along and across the radial directions, respectively.

These 1-D errors will propagate the uncertainty in the position of point A in two dimensions (area occupied by dashed lines in Fig. 1). These two sources of error will be compatible if their effects (the propagated errors) in the final location are of similar size or comparable ( $\Delta r \cong r\Delta\theta$ ) [18]. It is worthwhile to note that increasing the accuracy of any one (linear or angular) observation here will not increase the total accuracy significantly, as the error in the other observation still displaces the point. It is understood that the cost of resources involved in a project increases exponentially with their accuracy. This therefore necessitates selection of the resources (linear or angular observation in the above example and topographic data and sun algorithm in this paper) judiciously so their accuracies are compatible, thus leading to optimum cost in their use.

Financial cost (both fixed and operational) of all resources depends upon various heads and factors over the complete life cycle of the project. As high-precision or high-accuracy instruments (software and hardware) are costlier, therefore, aiming at higher accuracy certainly demands higher investments and efforts (computational and manual). This dictates the overall cost (initial cost+running cost), including the cost of data capture and sun position algorithms. Estimating, modeling, and minimizing the combined cost or total cost of two resources using corresponding cost indicators, especially when both are of different characteristics, is a critical and complicated task. Moreover, desired indicators of cost vary according to requirement and time span of a project. As a result, cost indicators are not available explicitly. Therefore, for all practical reasons, an approach of assuming simple cost function, which is inversely proportional to the precision of individual instruments and subjected to accuracy constraint, cannot be developed. Therefore, instead of adopting a mathematically based cost function, the cost is estimated by experience and heuristic methods considering fixed and running costs including the overheads of a project.

Cost of shadow determination, which may be estimated mathematically or heuristically, is subjected to the constraint that maximum error or precision ( $\sigma_{\max}$ ) obtained in shadow coordinates should be less than or equal to the maximum allowable error  $\eta$  (i.e.,  $\sigma_{\max} \leq \eta$ ). The following discussion derives the expressions of accuracy or maximum errors in shadow coordinates of a point represented by 3-D topographic data.

### B. Shadow Coordinates, Propagated Errors, Principal Components, and Compatibility

Point O with its geographical location  $(\lambda, \phi)$  known on the earth surface is an observer’s location where sun position (azimuth angle  $\theta$ , elevation angle  $\alpha$ ) is determined using any sun position model (Fig. 2). A right-handed 3-D Cartesian local geodetic (LG) coordinate system is centered at O with its Y- and Z-axis along geodetic north and ellipsoidal normal, respectively. Each object in 3-D is expressed by points  $(X, Y, Z)$  in LG system. The shadow of point A  $(X_A, Y_A, Z_A)$  is formed on

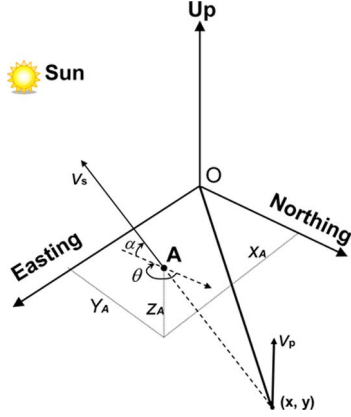


Fig. 2. Shadow formation of point A in LG plane.

the LG plane as  $(x, y)$ . Let  $\nu_s$  and  $\nu_p$  be the direction vectors of sun and LG plane.

Therefore, the shadow coordinates [19] are expressed as

$$\mathbf{X} = \mathbf{X}_A - \left( \frac{\nu_p^T \mathbf{X}_A}{\nu_p^T \nu_s} \right) \nu_s \quad (1)$$

where

$$\begin{aligned} \nu_s &= [\cos \alpha \sin \theta \quad \cos \alpha \cos \theta \quad \sin \alpha]^T \\ \nu_p &= [0 \quad 0 \quad 1]^T \\ \mathbf{X} &= [x \quad y \quad 0]^T; \mathbf{X}_A = [X_A \quad Y_A \quad Z_A]^T. \end{aligned}$$

Substituting values in (1) gives shadow coordinates as

$$x = X_A - \left( \frac{Z_A}{\tan \alpha} \right) \sin \theta \quad (2)$$

$$y = Y_A - \left( \frac{Z_A}{\tan \alpha} \right) \cos \theta. \quad (3)$$

For an accurate data or model, errors in variables are represented by precision (or variance) [20]. Consequently, propagated errors are shown by the following expressions (see the Appendix for details):

$$\sigma_x^2 = a_1 \sigma_{X_A}^2 + a_2 \sigma_{Y_A}^2 + a_3 \sigma_{Z_A}^2 + a_4 \sigma_\theta^2 + a_5 \sigma_\alpha^2 \quad (4)$$

$$\sigma_y^2 = b_1 \sigma_{X_A}^2 + b_2 \sigma_{Y_A}^2 + b_3 \sigma_{Z_A}^2 + b_4 \sigma_\theta^2 + b_5 \sigma_\alpha^2 \quad (5)$$

$$\sigma_{xy} = c_1 \sigma_{X_A}^2 + c_2 \sigma_{Y_A}^2 + c_3 \sigma_{Z_A}^2 + c_4 \sigma_\theta^2 + c_5 \sigma_\alpha^2 \quad (6)$$

where  $\sigma^2$  indicates the variance of a variable which is specified by the subscript. Coefficients  $a_1$ – $c_5$  are derived with details given in the Appendix.  $\sigma_x^2$  and  $\sigma_y^2$  are square values of the propagated random errors in the position of a shadow point in two orthogonal directions and also form an error ellipse. As stated earlier, the maximum error in shadow coordinates should not exceed the maximum allowable error ( $\eta$ ). Consequently, the maximum error in error ellipse ( $\sigma_{\max}$ ), which is equal to the first principal component value (FPCV or  $\sigma_{PC}$ ) should be less than or equal to maximum allowable error ( $\sigma_{PC} \leq \eta$ ). Expressions of principal components are listed in (11) in the Appendix.

Minimizing the total cost with the accuracy constraint ( $\sigma_{PC} \leq \eta$ ) will certainly provide the optimal solution. Prac-

tically, for a point in 3-D, accuracy ( $\sigma_{3D}$ ) is a function of precision in three axes  $X, Y$ , and  $Z$ . Similarly, the accuracy of sun model ( $\sigma_{SA}$ ) consists of precision of sun azimuth and sun elevation. Therefore, for all possible combinations of 3-D data acquisition technique and sun algorithms, the total cost will accordingly change. The FPCV and second principal component value (SPCV) represent the uncorrelated maximum and minimum errors of shadow coordinates in two orthogonal directions. Therefore, the ratio of SPCV and FPCV gives information about the shape of the error ellipse as higher value forms near the circular shape of ellipse and thus shows the uniformity or equality in errors in two orthogonal directions. Consequently, this ratio is an indicator of the positional compatibility.

Considering complicated and lengthy analytical expressions of FPCV and SPCV and relatively fewer combinations of 3-D data acquisition techniques and sun algorithms, it is found appropriate to investigate the results by plotting the curves for FPCV and the ratio of SPCV to FPCV against time in a day ( $t$ ).

Figs. 3–6 show the plots for FPCV and ratio of SPCV to FPCV versus time for LiDAR data ( $1 \sigma_{\text{accuracy}} = 20$  cm in  $X, Y$ ;  $15$  cm in  $Z$ ) and total station data ( $1 \sigma_{\text{accuracy}} = 1$  cm in  $X, Y$ , and  $Z$ ), respectively. Two arbitrary locations are chosen, first in Jaiselmer (Thar Desert in West India) and second in Nainitaal situated in the hills of Himalaya (North India). Curves for these locations are indicated by legend “Desert” and “Hill,” respectively. Geographical coordinates (longitude and latitude) of these locations in the WGS84 reference system are used as input to the ENEA algorithm for 1 October, 2010. Considering the sunrise and sunset at around 6 am and 6 pm, respectively, in the month of October at this location, curves are drawn from 8 am to 5 pm (8:00–17:00 hours) Indian Standard Time (IST or country time of India) at a time step of 6 min (0.1 h). This range is chosen as most of the solar devices are not expected to work beyond this duration. The height of the obstruction in this case is selected as 10 m, which is the average height of a three-story building. The ENEA sun position model [17] is used here for calculating the sun elevation and sun azimuth and, therefore, precision values of sun position obtained by Grena [17] are considered (viz.,  $\sigma_\alpha = 2.0''$ ;  $\sigma_\theta = 2.6''$ ).

It is evident from Figs. 3–6 that, for LiDAR data and Total Station data, the curves of FPCV and the ratio of SPCV to FPCV are concave and convex curves, respectively. Furthermore, the curve of FPCV and the curve of the ratio of SPCV to FPCV reach their minima and maxima, respectively, around the noon when the sun elevation approaches maximum values. At lower sun elevation angles (time closer to sun rise and sun set), for both combinations of 3-D data and sun algorithms, maximum error is not only high but the error ellipse also show biased or skewed behavior as SPCV to FPCV ratio becomes too low. At both locations, curves show similar characteristics. However, because of longitude difference, sun rises later at desert location and the curve for desert location show a non-linearly varying shift from the curve of the hill location.

The combination of LiDAR data and ENEA algorithm provide more error in shadow coordinates compared to other combination (ENEA with Total Station). In Figs. 3 and 5, the points of intersection of horizontal line indicating the maximum al-

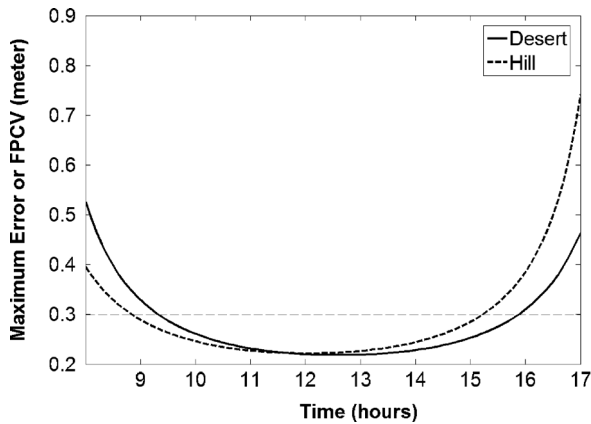


Fig. 3. FPCV curves for LiDAR data.

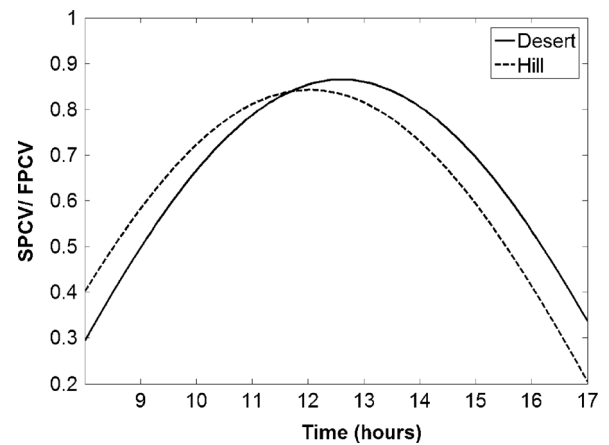


Fig. 6. Position compatibility (SPCV/FPCV) curves for Total Station data.

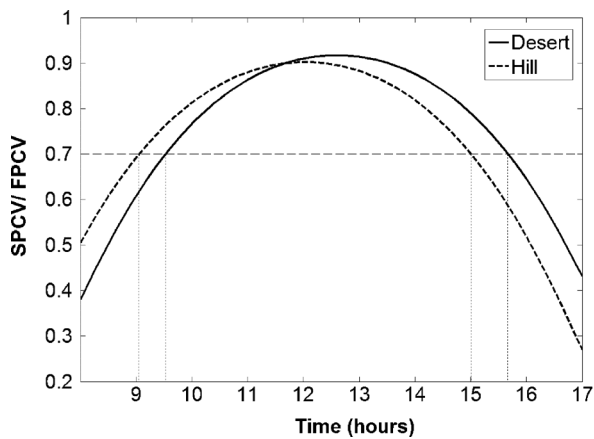


Fig. 4. Position compatibility (SPCV/FPCV) curves for LiDAR data.

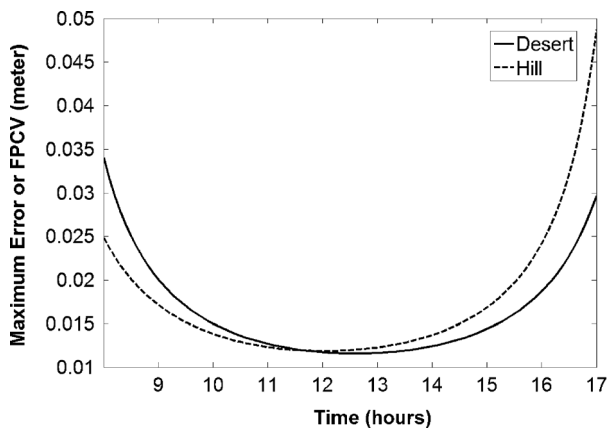


Fig. 5. FPCV curves for Total Station data.

lowable error ( $\eta$ ) with these curves can indicate the time zone or duration, for which the maximum errors are below the accuracy desired. Therefore, with LiDAR data, for a maximum allowable error of 0.3 m ( $\approx$  1 feet) in shadow coordinates, Fig. 3 reveals that 9:00 am to 3:00 pm duration (9:00–15:00 h) is appropriate as a combination of ENEA algorithm and LiDAR data can be used successfully for the location chosen in the hill. Similarly, for the desert location, the duration is from 9:30 am to

3:30 pm, showing an approximate shift of half an hour. However, this shift is not constant for other values of FPCV. Furthermore, during the same time, the ratio of SPCV to FPCV is better than 0.70. In other words, FPCV and SPCV are not off by more than 30% and thus ensure the positional compatibility by a factor of one third. On the other hand, the resultant maximum error in shadow coordinates due to the combination of ENEA algorithm and Total Station data is highly accurate (more than ten times than that of LiDAR data and ENEA algorithm). However, it performs poorer on the issue of positional compatibility for the same duration (9 am to 3 pm or 9:30 am to 3:30 pm).

In actual practice, the objects in a terrain will have different heights, and, thus, an average and maximum height should be considered. However, drawing the curves up to 1000 m showed the same pattern and similar values for these two curves. Therefore, the effect of height on the expected errors is negligible.

In practice, for user-defined maximum allowable error and eccentricity in positional compatibility, Figs. 3–6 can be used to determine the appropriate time duration for the chosen combination of sun algorithm and 3-D data at a particular geographical location. Thus, the proposed procedure can be utilized to assess the available 3-D data and sun algorithm for their positional and financial compatibility with given accuracy requirements.

### III. CONCLUSION

This paper has addressed the issue of the compatibility (financial, positional, and resource) of 3-D data and sun position model using the concept of error propagation. A compatibility criterion has been established using the terms derived from generic expressions of the principal components of errors ellipse assuming uncorrelated input variables of shadow coordinates. Plots drawn for the first principal component and the ratio of principal components during the daytime for a chosen obstruction height reveal the level and extent of maximum error and positional compatibility. Positional compatibility and maximum error analysis with cost considerations can help choose appropriate data and models thus minimizing the cost and efforts, instead of choosing these arbitrarily. For more realistic results of engineering significance, an additional approach of minimizing

the analytical cost function under constraint can be investigated for future research works.

#### APPENDIX

Error propagated in the shadow coordinates (4–6) can be determined by standard error propagation law [21]

$$\Sigma_{(xy)} = \mathbf{J}\Sigma_{(X_A Y_A Z_A \alpha \theta)}\mathbf{J}^T \quad (7)$$

where  $\mathbf{J}$  is the Jacobian matrix and  $\Sigma_{(X_A Y_A Z_A \alpha \theta)}$  is the covariance–variance matrix of five input variables  $(X_A, Y_A, Z_A, \alpha, \theta)$ . As 3-D data and the sun position algorithm are independent and further assuming uncorrelated input variables,  $\Sigma_{(X_A Y_A Z_A \alpha \theta)}$  is a diagonal matrix consisting of variances only. Matrix  $\mathbf{J}$  is written as

$$\mathbf{J} = \begin{bmatrix} \frac{\partial x}{\partial X_A} & \frac{\partial x}{\partial Y_A} & \frac{\partial x}{\partial Z_A} & \frac{\partial x}{\partial \alpha} & \frac{\partial x}{\partial \theta} \\ \frac{\partial y}{\partial X_A} & \frac{\partial y}{\partial Y_A} & \frac{\partial y}{\partial Z_A} & \frac{\partial y}{\partial \alpha} & \frac{\partial y}{\partial \theta} \end{bmatrix}$$

where

$$\begin{aligned} \frac{\partial x}{\partial X_A} &= 1 \\ \frac{\partial x}{\partial Y_A} &= 0 \\ \frac{\partial x}{\partial Z_A} &= \frac{-\sin \theta}{\tan \alpha} \\ \frac{\partial x}{\partial \alpha} &= \frac{Z_A \sin \theta}{\sin^2 \alpha} \\ \frac{\partial x}{\partial \theta} &= \frac{-Z_A \cos \theta}{\tan \alpha} \\ \frac{\partial y}{\partial X_A} &= 0 \\ \frac{\partial y}{\partial Y_A} &= 1 \\ \frac{\partial y}{\partial Z_A} &= \frac{-\cos \theta}{\tan \alpha} \\ \frac{\partial y}{\partial \alpha} &= \frac{Z_A \cos \theta}{\sin^2 \alpha} \\ \frac{\partial y}{\partial \theta} &= \frac{Z_A \sin \theta}{\tan \alpha} \end{aligned}$$

Substituting the values in (7) gives the diagonal and off-diagonal elements (variances and covariance of shadow coordinates) of the resultant matrix as

$$\sigma_x^2 = a_1\sigma_{X_A}^2 + a_2\sigma_{Y_A}^2 + a_3\sigma_{Z_A}^2 + a_4\sigma_\alpha^2 + a_5\sigma_\theta^2 \quad (8)$$

$$\sigma_y^2 = b_1\sigma_{X_A}^2 + b_2\sigma_{Y_A}^2 + b_3\sigma_{Z_A}^2 + b_4\sigma_\alpha^2 + b_5\sigma_\theta^2 \quad (9)$$

$$\sigma_{xy} = c_1\sigma_{X_A}^2 + c_2\sigma_{Y_A}^2 + c_3\sigma_{Z_A}^2 + c_4\sigma_\alpha^2 + c_5\sigma_\theta^2 \quad (10)$$

where  $\sigma^2$  and  $\sigma$  indicate the variance and covariance of variables which are specified by the subscripts. Coefficients from  $a_1$  to  $c_6$  are as follows:

$$\begin{aligned} a_1 &= 1 \\ a_2 &= 0 \\ a_3 &= \left( \frac{\sin^2 \theta}{\tan^2 \alpha} \right) \\ a_4 &= \left( \frac{Z_A^2 \sin^2 \theta}{\sin^4 \alpha} \right) \end{aligned}$$

$$a_5 = \left( \frac{Z_A^2 \cos^2 \theta}{\tan^2 \alpha} \right)$$

$$b_1 = 0$$

$$b_2 = 1$$

$$b_3 = \left( \frac{\cos^2 \theta}{\tan^2 \alpha} \right)$$

$$b_4 = \left( \frac{Z_A^2 \cos^2 \theta}{\sin^4 \alpha} \right)$$

$$b_5 = \left( \frac{Z_A^2 \sin^2 \theta}{\tan^2 \alpha} \right)$$

$$c_1 = 0$$

$$c_2 = 0$$

$$c_3 = \left( \frac{\sin 2\theta}{2 \tan^2 \alpha} \right)$$

$$c_4 = \left( \frac{Z_A^2 \sin 2\theta}{2 \sin^4 \alpha} \right)$$

$$c_5 = \left( \frac{-Z_A^2 \sin 2\theta}{2 \tan^2 \alpha} \right).$$

The square of the principal components values  $\sigma_{PC}$  of the propagated variance are given by [22]

$$\sigma_{PC}^2 = \left( \frac{\sigma_x^2 + \sigma_y^2}{2} \right) \pm \sqrt{\left( \frac{\sigma_x^2 - \sigma_y^2}{2} \right)^2 + \sigma_{xy}^2}. \quad (11)$$

#### ACKNOWLEDGMENT

The authors would like to thank R. Grena, ENEA—Centro Ricerche Casaccia, Rome, Italy, for useful discussions about the ENEA algorithm. The comments of the reviewers helped to improve the content of the revised paper.

#### REFERENCES

- [1] A. Hadhazy, "Power plants: Artificial trees that harvest sun and wind to generate electricity," *Scientific Amer. Mag.* Nov. 5, 2009 [Online]. Available: <http://www.scientificamerican.com/article.cfm?id=artificial-trees-harvest-sun-and-wind-energy#comments>
- [2] D. Despommier, "Growing skyscrapers: The rise of vertical farms," *Scientif. Amer. Mag.* Nov. 5, 2009 [Online]. Available: <http://www.scientificamerican.com/article.cfm?id=the-rise-of-vertical-farms>
- [3] E. Zell, J. Engel-Cox, R. Eckman, and P. Stackhouse, "Application of satellite sensor data and models for energy management," *IEEE J. Sel. Topics Appl. Earth Observ.*, vol. 1, no. 1, pp. 5–17, Mar. 2008.
- [4] R. Perez, M. Taylor, T. Hoff, and J. P. Ross, "Reaching consensus in the definition of photovoltaics capacity credit in the USA: A practical application of satellite-derived solar resource data," *IEEE J. Sel. Topics Appl. Earth Observ.*, vol. 1, no. 1, pp. 28–33, Mar. 2008.
- [5] E. Lorenz, J. Hurka, D. Heinemann, and H. G. Beyer, "Irradiance forecasting for the power prediction of grid-connected photovoltaic systems," *IEEE J. Sel. Topics Appl. Earth Observ.*, vol. 2, no. 1, pp. 2–10, Mar. 2009.
- [6] X. Zhang, S. Liang, K. Wang, L. Li, and S. Gui, "Analysis of global land surface shortwave broadband albedo from multiple data sources," *IEEE J. Sel. Topics Appl. Earth Observ.*, vol. 3, no. 3, pp. 296–305, Sep. 2010.
- [7] M. Sári, T. Huld, E. D. Dunlop, and T. Cebecauer, "Geographic aspects of photovoltaics in europe: Contribution of the PVGIS website," *IEEE J. Sel. Topics Appl. Earth Observ.*, vol. 1, no. 1, pp. 34–41, Mar. 2008.
- [8] M. Sári, T. Cebecauer, and A. Skoczek, "SolarGIS: Solar data and on-line applications for PV planning and performance assessment," presented at the 26th Eur. Photovoltaics Solar Energy Conf., Hamburg, Germany, 2011.

- [9] R. Dubayah and P. M. Rich, "Topographic solar radiation model for GIS," *Int. J. Geographic Inf. Syst.*, vol. 9, pp. 405–419, 1995.
- [10] A. Jochem, B. Hoffeb, M. Hollausb, and M. Rutzinger, "Object detection in airborne lidar data for improved solar radiation modeling in urban areas," *Int. Archives of Photogrammetry, Remote Sensing and Spatial Inform. Sciences*, vol. 38, pp. 1–9, 2009, (part 3/W8).
- [11] A. Jochem, V. Wichmann, and B. Höfle, "Point cloud based solar radiation modeling," in *SAGA Third Degree, Hamburger Beiträge zur Physischen Geographie und Landschaftsökologie-Heft 20*, 2009, vol. 21, pp. 1–9.
- [12] G. Aguiaro, F. Remondino, G. Stevanato, R. D. Filippi, and C. Furlanello, "Estimation of solar radiation building roofs in mountainous areas," *Int. Archives of Photogrammetry, Remote Sensing and Spatial Inform. Sciences*, vol. 38, pp. 155–160, 2011, (part 3/W 22).
- [13] P. Redweik, C. Catita, and M. C. Brito, "3D local scale solar radiation model based on urban lidar data," presented at the ISPRS Hannover Workshop 2011 High-Resolution Earth Imaging for Geospatial Information, Hannover, Germany, 2011.
- [14] M. Blanco-Murile, D. C. Alarcon-Padilla, T. Lopez-Moratalla, and M. Lara-Coira, "Computing the solar vector," *Solar Energy*, vol. 70, no. 5, pp. 431–441, 2001.
- [15] J. J. Michalsky, "The astronomical almanac's algorithm for approximate solar position (1950–2050)," *Solar Energy*, vol. 40, no. 3, pp. 227–235, 1988.
- [16] I. Reda and A. Andreas, "Solar position algorithm for solar radiation applications," *Solar Energy*, vol. 76, no. 5, pp. 577–589, 2004.
- [17] R. Grena, "An algorithm for the computation of the solar position," *Solar Energy*, vol. 82, no. 5, pp. 462–470, May 2008.
- [18] C. A. Herubin, *Principles of Surveying*. Englewood Cliffs, NJ: Prentice-Hall, 1982, ch. 2, pp. 23–37.
- [19] R. Budin and L. Budin, "A mathematical model for shading calculations," *Solar Energy*, vol. 29, no. 4, pp. 339–349, 1982.
- [20] J. R. Taylor, *An Introduction to Error Analysis*. Sausalito, CA: University Sci., 1997, ch. 4, pp. 93–120.
- [21] E. M. Mekhail, *Observations and Least Squares*. New York: IEP-A Dun Donnelley, 1976, ch. 4, pp. 72–97.
- [22] E. M. Mekhail and G. Gracie, *Analysis and Adjustment of Survey Measurements*. New York: Van Nostrand Reinhold, 1981, ch. 8, pp. 197–235.



**Ajay Dashora** born in Jaipur, Rajasthan, India, on October 7, 1978. He received the B.E. degree in civil engineering from the M.B.M. Engineering College, Jodhpur, India, in 2001, and the M.Tech. degree in geoinformatics from Indian Institute of Technology Kanpur, Kanpur, India, in 2005, where he is currently working toward the Ph.D. degree.

During his M.Tech. work, he worked in the area of physical modeling of corona satellite images. Before joining the Ph.D. program in January 2009, he was a Research Associate in the area of flood modeling, as a Senior Engineer in automobile industry, and as a Regional Data Sourcing Manager in navigation industry. His current research interests include physical modeling, use of evolutionary algorithms in remote sensing, integration of remote sensing data acquisition methods and techniques using aerial platforms, and application of remote sensing techniques.

Mr. Dashora received the best research paper award from Indian Society of Remote Sensing in 2006 for devising a better and cost effective technique for planning and collection of ground control points for historical images and photographs.



**Bharat Lohani** received the Ph.D. degree from the University of Reading, Reading, U.K., in LiDAR technology and environmental sciences, in 1999.

He is currently an Associate Professor with the Indian Institute of Technology Kanpur, Kanpur, India, where he has been since 2002. He has interest in teaching and research in the domain of laser scanning-data capture, processing and application development. He has published papers in the area of extraction of channel networks, buildings from LiDAR data. He has developed model for predicting

GPS-GDOP using LiDAR data and URP. He has been behind the development of LiDAR Simulator.

Dr. Lohani is currently Co-Chair with ISPRS WG V-2 and a Fellow with the Institution of Surveyors, India.